ADVANCED MULTI-EVAPORATOR LOOP THERMOSYPHON

M. Mameli[a*], D. Mangini[b], G. F. T. Vanoli[c], L. Araneo[c], S. Filippeschi[a], M. Marengo[b,d]

[a]Università di Pisa, DESTEC, Largo Lazzarino 2, 56122 Pisa, Italy

[b]Università di Bergamo, Viale Marconi 5, 24044 Dalmine (BG), Italy

[c]Politecnico di Milano, Dipartimento di Energia, Via Lambruschini 4A, 20158 Milano, Italy

[d]University of Brighton, School of Computing, Engineering and Mathematics, Lewes Road, Brighton BN2 4GJ, UK.

[*]Corresponding author: mauro.mameli@ing.unipi.it

ABSTRACT

A novel prototype of multi-evaporator closed loop thermosyphon is designed and tested at different heaters position, inclinations and heat input levels, in order to prove that a peculiar arrangement of multiple heaters may be used in order to enhance the flow motion and consequently the thermal performance. The device consists in an aluminum tube (Inner/Outer tube diameter 3.0 mm/5.0 mm), bent into a planar serpentine with five U-turns and partially filled with FC-72, 50% vol. The evaporator zone is equipped with five heated patches (one for each U-turn) in series with respect to the flow path. In the first arrangement, heaters are wrapped on each bend symmetrically, while in the second layout heaters are located on the branch just above the U-turn, non-symmetrical with respect to the gravity direction, in order to promote the fluid circulation in a preferential direction. The condenser zone is cooled by forced air and equipped with a 50 mm transparent section for the flow pattern visualization. The non-symmetrical heater arrangement effectively promotes a stable fluid circulation and a reliable operation for a wider range of heat input levels and orientations with respect to the symmetrical case. In vertical position, the heat flux dissipation exceeds the pool boiling heat transfer limit for FC-72 by 75% and the tube wall temperatures in the evaporator zone are kept lower than 80 °C. Furthermore, the heat flux capability is up to five times larger with respect to the other existing wickless heat pipe technologies demonstrating the attractiveness of the new concept for electronic cooling thermal management.

Keywords: Thermosyphon, wickless heat pipes, passive heat device, non-symmetrical heating, flow pattern visualization.

1 INTRODUCTION

According to the more optimistic scenario (Representative Concentration Pathway 2.6) expected by the Intergovernmental Panel on Climate Changes [1], an average 50% reduction of greenhouse emissions is required by 2050, relative to 1990 levels, in order to obtain their substantial decline thereafter. The energy consumption and the efficiency of several industrial processes are nowadays under the magnifying glass. For instance, recent studies on information technology data centers showed that the rate of increase of their energy consumption is growing faster than several other major industries [2]. In particular, due to the miniaturization of electronic components and the consequent increase of power densities, the electric energy required for electronic thermal management contributes to a large amount with respect to the total (up to 50% for data centers) Indeed, heat dissipation is mainly achieved through active systems, such as forced convection liquid loops or fans above the heat sinks directly mounted on the boards. In this context, the implementation of passive two-phase heat transfer devices would be a breakthrough solution: being very efficient heat flux spreaders, two-phase passive devices are capable of reducing the very high heat powers per unit of surface generated by the electronics in contact with the evaporator, to the lower heat fluxes that may be dissipated on larger and more accessible surfaces in the condenser zone. This allows to substantially reduce the fan energy consumption in the case of optimized natural or mixed convection coolers.

Two-phase heat transfer loops have always been attractive for their compactness, high performance and because they are thermally driven. While the last decades witnessed the overwhelming spread of the heat pipe technology under various forms such as grooved and sintered heat pipes, loop heat pipes and capillary pumped loops, the interest in wickless, gravity driven technologies, namely the Two-Phase Thermo-Syphons (TPTS), never damped out. The capability to transport heat at high rates over appreciable distances, without any requirement for external pumping devices, the low cost, durability and relatively simpler modeling/design process make this technology very attractive for many thermal management applications. Indeed, TPTS have been investigated in plenty of fields such as: nuclear plants [3], energy systems [4], solar heat recovery [5,6,7], air conditioning [8], electronic cooling in avionics [9] and in railway traction [10]. The typical TPTS [11] consists of a single envelope where the heat-receiving (evaporator) zone is usually filled with the liquid phase and it is located below the heat rejecting (condenser) zone. As the evaporator zone is heated up, the liquid starts boiling and vapor rises and condenses on the walls in the heat-rejecting zone. The liquid film flows down the walls by gravity to the evaporator zone, counter-current the vapor. At high heating power input, because of the correspondingly large mass flow rate of the vapor, the liquid-vapor interfacial shear stress becomes increasingly relevant. Once the interfacial shear force overcomes the gravitational force on the liquid film, the liquid flow may be reversed and the flooding limit is reached. Many novel designs have been proposed to overcome the flooding limit, which include an internal physical barrier along the adiabatic section by-pass line for liquid return, also known as a cross-over flow separator [12]. The main advantage of these designs is that the liquid and vapor flows have partially separated passages, which can result in a higher flooding-limited heat transfer capacity. Another possibility to separate phases and increase the device performance is to create a closed circuit. In such a loop, the fluid is forced to circulate in a preferential direction by the coupled effect of vapor pressure and gravitational force as thoroughly described by [13]. Thanks to the relatively small cross section with respect to the standard TPTS, the expanding vapor phase pushes batches of fluid (both liquid and vapor) towards the condenser section. In the cooled zone, vapor condenses and the tube is completely filled by the liquid phase that is driven back to the evaporator by gravity. This particular fluid flow motion is better known as “bubble lift” principle [14] and shown in figure 1. Defining the capillary length as $l_c = \sqrt{\sigma / g(\rho_l - \rho_v)}$, the looped TPTS based on the “bubble lift” concept fills the gap between the capillary dominated systems (Pulsating Heat Pipes $d < 2l_c$ [15,16]) and the buoyancy dominated systems (Counter-flow thermosyphons $d > 19l_c$ [14]).

In the present work, the concept of single closed loop thermosyphon is revolutionized in a twofold manner: first, the tube is bent in a serpentine manner introducing multiple heated and cooled zones; second, the heating patches are strategically switched from a symmetrical to a non-symmetrical layout in order to enhance the fluid flow circulation of in a preferential direction. This creates a novel device that might be named as Multi-Evaporator Loop Thermosyphon (MELT). Since the fluidic path is unique and the heated and cooled zones are in series, the present device works in a different way as the parallel assessments [17, 18] previously studied in literature. In the same time, it doesn't lose its construction simplicity. The studied one in this paper consists of an aluminum tube, which is bent in a serpentine and partially filled with FC-72. Based on the current approach, this device represents a Multi-Evaporator Loop Thermosyphon (MELT). Experimental results show that the non-symmetrical location of the heated zones is beneficial with respect to the symmetrical both in terms of fluid circulation enhancement and heat flux removal. Thanks to the self-sustained fluid circulation, the maximum heat flux abundantly exceeds the standard pool boiling critical flux by up to 75%, and largely improves upon the heat input range capability of standard thermosyphons [19] and other promising wickless heat pipe technologies [20] operated with fluorinerts.

Table 1 resumes the advantages and drawbacks of the wickless heat pipe technologies according to some general merit parameters such as performance, cost, modeling. Despite the dependency on gravity assistance and the actual lack of design tools, the MELT technology represents a good alternative to the standard thermosiphon where more geometrical flexibility is needed and a good alternative to the Pulsating Heat Pipe where higher heat flux capability and compactness are requested.

2 EXPERIMENTAL SET UP AND PROCEDURE

The proposed cooling device is made of an aluminum tube (Inner/Outer tube diameter 3.0 mm/5.0 mm) bent into a planar serpentine with five U-turns at the evaporator (curvature radius 7.5 mm) and ten parallel channels. Two "T" junctions, respectively devoted to the vacuum and filling procedures and fluid pressure measurement (Kulite®, XCQ-093, 1.7 bar Absolute), also allow to install a 50 mm glass tube for the purpose of visualization, as shown in Figure 2a.

A low vapor-pressure glue (Varian Torr Seal®) seals together the aluminum tube, the "T" junctions and the glass tube. Sixteen "T" type thermocouples (bead diameter 0.2 mm, ± 0.3 K) are located on the thermosyphon external tube wall: ten in the evaporator zone and six in the condenser zone, while a PT 100 sensor (Class B sensor RS®) is utilized to measure the ambient temperature as illustrated in Figure 2a, while Figure 2b shows an exploded view of the entire test cell.

The thermosyphon is firstly evacuated by means of a Varian® DS42, TV81-T vacuum system down to 10^{-6} mbar. Before filling up, the incondensable gases are first removed by multiple boiling and vacuum cycles in a secondary tank, as described by Henry et al. [21]. Finally, the system is filled up with the working fluid (FC-72) utilizing a filling ratio of 0.50 ± 0.03, corresponding to a liquid volume of 8.3 ml. The difference between the actual fluid pressure inside the tube and its saturation pressure, at the ambient temperature, gives an indication of the incondensable gas content. For the present case, this difference is less than the pressure transducer accuracy (800 Pa).

The complete view of the experiment rig with its main components, is shown in Figure 3. A power supply (GWInstek® 6006A) is connected to the evaporator heaters, providing a heating power input up to 260 W.

A compact camera (Ximea®, MQ013MG-ON objective: Cosmicar/Pentax® C2514-M) records the flow patterns within the glass tube. By cropping the recorded region of interest to the glass tube only, the camera can acquire images at up to 450 fps with a resolution of 1280x162 pixels (corresponding to a spatial resolution of 25 pixels/mm). The thermocouples, the PT-100 and the pressure transducer outputs are recorded by a data acquisition system (NI-cRIO-9073®, NI-9214®, NI-9215®, NI-9217®) at 16 Hz. A video sequence (10 seconds at 450 fps) is recorded during each tested combination of heat input power and inclination angle. The video acquisition starts 13 minutes after each heat input power variation in order to ensure pseudo-steady state conditions have been reached completely. The cooling device, the thermocouples, the PT-100, the pressure transducer, the heating and cooling system as well as the visualization system are installed on a structure that can be easily tilted from the vertical position (bottom heat mode) to the horizontal.

2.1 Evaporator zone

Five electrical heaters (Thermocoax® Single core 1Nc Ac, 0.5 mm O.D., 50 Ω/m, each wire is 720 mm long) are wrapped around the tube in the evaporator section. Two different arrangements of the heaters are tested:

1. Symmetrical heating: the wires are located on each bend symmetrically, each one covering 40 mm of the tube axial length, corresponding to a wall to fluid heated area of 3.8 cm^2, as shown in Fig. 4a;
2. Non-symmetrical heating: the wires are positioned on the branches just above the U-turns, non-symmetrically with respect to the gravity direction, each one covering 20 mm of the tube axial length, corresponding to a wall to fluid heated area of 1.9 cm^2, as shown in Fig. 4b. As a consequence, if the same power is provided to both the configurations, the wall to fluid heat flux of non-symmetrical configuration will be twice the heat flux in the symmetrical case, as shown in Table 2.

The power supply provides a heating power input up to 260 W, corresponding to a wall to fluid heat flux input of 13.75 W/cm^2 for the symmetrical case and 27.5 W/cm^2 for the non-symmetrical. Steady state conditions can be reached in approximately three minutes due to the low thermal inertia of such heating system.

It is worthwhile to note that each branch in the evaporator zone is equipped with one thermocouple: for the symmetrical case (Figure 4a) all of them are located 1 mm just above the heating wire. For the non-symmetrical layout, since the thermocouple array is shifted up by 10 mm, only one thermocouple per curve (TC-1, 3, 5, 7, 9 in figure 2a) is close to the heater but this is still sufficient to characterize the evaporator zone.

2.2 Condenser zone

In order to increase the condenser surface, the device is embedded between a heat sink and a back plate (Figure 5a) where circular cross section channels are milled. The thermosyphon is cooled down by means of two air fans (Sunon® PMD1208PMB-A), positioned just above the heat sink (165 mm total length), as shown in Figure 5b. The thermal contact between the heat sink, the aluminum back plate and the enclosed thermosyphon is enhanced by the use of thermal conductive paste (RS® Heat Sink Compound). All the tests are performed at controlled ambient temperature (20 °C ± 3 °C).

3 RESULTS

The experimental campaign is carried out in order to compare the two different heater arrangements by identifying:

- the temporal evolution of the tube temperatures and local fluid pressure at the condenser at different heat flux levels;
- the device thermal performance and operational limits in terms of heat input levels and orientation with respect to the vertical position: 75°, 60°, 45°, 30°, 15°, 2.5°, 0° (Horizontal);
- the operational regimes in terms of fluid motion;

For each inclination, the heater input power is increased in multiples of 10 W steps, with finer detail in the lower power region in order to detect the start up heat flux. Power is furtherly increased with coarser heat input levels in order to reach the Critical Heat Flux (CHF) and, consequently, the evaporator dry-out condition. After the sudden increase of the evaporator temperatures due to the dry-out condition, the heating power is reduced following the same heating level pattern.

Each power step is maintained for at least 15 up to 16 minutes so that the system can reach a pseudo-steady state condition, the equivalent thermal resistance is evaluated for the last 4 minutes of each power step by means of equation 1:

$$R_{th} = \frac{\bar{T}_e - \bar{T}_c}{\dot{Q}} \qquad 1)$$

$$\bar{T}_e = \frac{1}{5}\sum_{i=1}^{5} T_{e,i} \qquad 2)$$

$$\bar{T}_c = \frac{1}{6}\sum_{i=1}^{6} T_{c,i} \qquad 3)$$

$$\dot{Q} = I^2 R_{el} \qquad 4)$$

Where $\bar{T}_e$, $\bar{T}_c$ are the evaporator and condenser average temperature; $T_{e,i}$ and $T_{c,i}$ the evaporator and condenser temperatures related respectively to TC1, TC3, TC5, TC7, TC9 (evaporator) and TC10, TC11, TC12, TC13, TC14, TC15 (condenser). $\dot{Q}$ is the total heat power provided to the heaters; I the controlled current supplied by the power supply, R_{el} the total electrical resistance of the heaters, R_{th} the equivalent thermal resistance.

According to Moffat [22], the uncertainties of the above quantities can be evaluated as follow. In particular the partial derivatives are evaluated to the corresponding variable average values.

$$\delta R_{th} = \sqrt{\left(\frac{\partial R_{th}}{\partial \bar{T}_e}\delta \bar{T}_e\right)^2 + \left(\frac{\partial R_{th}}{\partial \bar{T}_c}\delta \bar{T}_c\right)^2 + \left(\frac{\partial R_{th}}{\partial \dot{Q}}\delta \dot{Q}\right)^2} \qquad 5)$$

$$\delta \bar{T}_e = \sqrt{\frac{1}{5}\sum_{i=1}^{5}\left(\frac{\partial \bar{T}_e}{\partial T_{e,i}}\delta T_{e,i}\right)^2} \qquad 6)$$

$$\delta \bar{T}_c = \sqrt{\frac{1}{6}\sum_{i=1}^{6}\left(\frac{\partial \bar{T}_c}{\partial T_{c,i}}\delta T_{c,i}\right)^2} \qquad 7)$$

$$\delta\dot{Q} = \sqrt{\left(\frac{\partial\dot{Q}}{\partial I}\delta I\right)^2 + \left(\frac{\partial\dot{Q}}{\partial R_{el}}\delta R_{el}\right)^2} \quad 8)$$

Where $\delta\dot{Q}$ and δR_{th} are the uncertainty of the power supplied and the equivalent thermal resistance. δI, δR_{el} are the uncertainties of the current supplied and the total electrical resistance of the heaters, taken from datasheet (see table 3 a), while $\delta\overline{T}_e$, $\delta\overline{T}_c$, $\delta T_{e,i}$ and $\delta T_{c,i}$ are the evaporator and condenser average temperatures. The uncertainties $\delta T_{e,i}$ and $\delta T_{c,i}$ are evaluated by their fixed component δT_{ds} taken from the acquisition system datasheet (Table 3 a), and their noise component related to the measurement standard deviations (σ_e, σ_c).

$$\delta T_{e,i} = \sqrt{\delta T_{ds}{}^2 + \left(2\sigma_e\right)^2} \quad 9)$$

$$\delta T_{c,i} = \sqrt{\delta T_{ds}{}^2 + \left(2\sigma_c\right)^2} \quad 10)$$

The uncertainties related to the heat input level, the average temperatures and the overall thermal resistance have been calculated for the non-symmetrical configuration, vertical case, in order to cover the whole heat input range (Table 3b). The relative maximum uncertainty for the heat input level (5.8%) and the overall thermal resistance (10.55%) has been detected at the lower heat input level.

3.1 Thermal characterization in vertical position

The temporal evolution of the tube wall temperatures and of the fluid pressure is shown both for the symmetrical case (Figure 6a) and the non-symmetrical case (Figure 6b). The secondary x–axis (upper side) indicates the total heating power as well as the corresponding heat input flux levels. Odd number thermocouples (TC1, TC3, TC5, TC7, TC9) are labeled with red/yellow lines while even (TC0, TC2, TC4, TC6, TC8) are represented with pink colors. The temperatures recorded in the condenser zone are illustrated with blue color lines (TC10, TC11, TC12, TC13, TC14, TC15); the ambient temperature "TC_{env}" is shown in green; finally, the fluid pressure "P" temporal trend is displayed (secondary y- axis) in dark grey color. Such representation allows the detection of the operational regimes namely the start-up when the temperature oscillation is recognizable in a few branches; the complete activation when the fluid starts to flow through all the channels, and the circulating regime when the fluid flows in a preferential direction. It is worthwhile to mention that the dry-out limit was not reached in both cases, due to the power supply capability.

During the first heat input level the fluid is not moving, as evidenced by the smooth pressure signal, and heat is transferred mostly by pure conduction along the tubes. For this reason, even small differences in the thermal contact between the five heating wires and the tube portions can cause a large temperature spread within the evaporator zone. At the lower heating levels only a single or a few heated zones reach the superheating level required to activate the phase change process. Boiling may indeed occur locally in a single evaporator portion, causing the temperature drop only for the two corresponding temperature measurements as shown in figure 7a.

This partial start-up occurs at 20 W both in the symmetrical and non-symmetrical case. Only when all the heated zones are above the superheating temperature level, the full activation occurs and all the temperature trends drop down as shown in figure 7b.

The full activation occurs at 40 W for both the configurations but, interestingly, the non-symmetrical case switches to the circulating mode immediately after, as detected by the fluid visualization study (Fig. 8a and 8b), and from the tube wall temperature trend recorded just before and after the glass tube section (TC14 and TC15) as shown in figures 8b and 8d.

In the symmetrical case, after the complete activation, the fluid inside the transparent section does not follow a preferential direction as shown in Figure 8a. The temperature measurements at the extremities of the transparent section reveal the occurring of frequent flow reversals: TC14, TC15 come close to each other depending on the actual flow direction (Fig. 6b). Only when the heat input level reaches 210 W the two temperatures diverge and the fluid starts moving in a preferential direction while maintaining an oscillating component. As expected, in the non-symmetrical case fluid circulation is detected immediately after the full activation. (Figure 6c). From 40 W to 260 W, the temperature recorded by TC14 is indeed always higher than the one recorded by TC15 (an example of flow circulation at 120W is shown in Figure 8d). Furthermore, it is worthwhile to focus the attention on the fluid pressure trend in relationship with the fluid motion characteristics. Despite the pressure transducer being plugged perpendicular to the flow path and therefore unable to detect the fluid direction but only the fluid momentum changes, a high pressure oscillation amplitude (Fig. 8b), can be correlated both to high accelerations/decelerations, and flow reversals.

Thanks to the peculiar position of the heaters, the combined effect of vapor bubble-lift and gravity helps the fluid rise up from the heated tubing sections and descend into the cooled sections respectively, as shown in Figure 9.

Inside the heated branches (up-headers), the fluid batches of both vapor and liquid phase are lifted up from the evaporator to the condenser, by means of the expanding vapor bubbles. The gravity head along the adjacent branches (down-comers) assists the return of the condensed fluid from the condenser down to the evaporator zone. Given that, for evaporator length to tube diameter ratios ($l_e/d_{in}>5$), the boiling limit is the less severe among the operational constraints (i.e. entrainment limit) for a standard thermosyphon [23], the general pool boiling CHF for FC-72 can be considered as the ideal maximum heat flux achievable. Furthermore, in order to compare the MELT technology with the closed Thermosyphon, the maximum heat flux is evaluated by means of existing correlations developed for the TS (Table 4). The CHF is calculated for each case by means of equation 2 [24] considering the thermophysical properties of FC-72 at 80°C:

$$q''_{CHF} = Ku\Delta h_{lv}\rho_v^{0.5}\left[\sigma g\left(\rho_l - \rho_v\right)^{0.25}\right] \quad (2)$$

The obtained values can be compared to the experimental data from other literature (Table 5). In particular, the Pool boiling CHF obtained by Jung et al. [26] agrees well with the prediction by Zuber [25] and also the Maximum heat flux achieved by the Closed Thermosyphon tested by Jouhara and Robinson [19] matches with the one predicted by Katto [26] and also by Pioro and Voroncova [27]. In order to appreciate the increase of heat flux capability of the MELT technology with respect to TS and to another promising wickless heat pipe known in literature as Pulsating Heat Pipe [20], Table 5 also contains the technical data of three very similar experimental cases linked to the mentioned technologies. It is worthwhile to notice that for the experimental cases **q"$_{\mathbf{CHF}}$** is the maximum heat flux achievable with a stable operation before the occurrence of the thermal crisis. In order to give an idea of the heat flux capability enhancement due to the circulation of the fluid (MELT) with respect to the other cases, the last row of Table 5 summarizes the percentage improvement.

A three times increase with respect to the Pool Boiling limit suggests that the actual working mode of the MELT technology is somehow closer to the flow boiling principles, even though the mass flow rate is rather than constant. In such new framework, further work must is needed in order to provide a suitable correlation for evaluating the CHF. Interestingly the MELT technology is also filling some gaps still present in the promising PHP technology: the smart use of gravity assistance not only contributes to obtain larger heat flux capabilities but also to stabilize the circuit operation, making it more reliable and predictable.

3.2 Effect of the orientation

Beyond the characterization in vertical position, further tests at φ = 75°, 60°, 45°, 30°, 15°, 2.5° and the horizontal position (0°) are performed in order to evaluate the effect of inclination on the thermal hydraulic behavior. Results are summarized in terms of equivalent thermal resistance shown in Figure 10. In horizontal orientation, since the phase distribution is completely stratified, the liquid phase resides in the lower half of the pipe while the vapor phase in the upper one. Consequently, there is no mean of macroscopic fluid motion for all the tested heat input levels, proving that even a small gravitational assistance is required to activate the device. In order to allow the liquid to distribute itself evenly among the curves, the device was placed in horizontal position before setting it to the desired inclination. For all the four tests performed in a horizontal orientation, the equivalent thermal resistance is constant and sets to the highest value of 0.8 K/W, confirming that the heat transfer is mainly due to conduction within the tube wall and the fluid itself. This trend is taken as reference point in order to understand whether the device is working or not.

Figure 10a and 10b show the equivalent thermal resistance during the power-up phase for the symmetrical case and for the non-symmetrical case respectively, while Figure 8c and 8d display the equivalent thermal resistance during the power down phase. It is immediately clear that when the device is heated up starting from ambient temperature there is no univocal dependence between the start-up heat input level and the device orientation. In fact, one could expect that the device start-up may occur at lower heat input levels for lower inclinations but, looking at Figure 10a and 10b, it is evident that the start-up heat input ranges randomly from 20 W to 60 W. This start-up issue, detected also for another two-phase passive loop, namely the Closed Loop Pulsating Heat Pipe when gravity assisted [20], not only depends on the heat input level and on the wall to fluid superheat but also on the initial distribution of liquid and vapor phases inside the channels and must be furtherly investigated. On the other hand, during the power-down case (Fig. 10c and 10d), the fluid motion remains active down to 30 W for all the inclinations, meaning that the liquid phase is pushed back to the condenser more efficiently when the gravity effect is coupled with fluid inertial effects. This is also confirmed for medium-low power inputs by the fact that all the curves collapse into a narrower band with respect to the power-up case. The technical implications of the above outcome are positive: once the device is fully activated, a subsequent decrease of the heat flux below the first start up level does not compromise the device operation.

The only peculiar trend among all the orientations is detected when the device is just slightly tilted with respect to the horizontal position (2.5°); this small gravity head is sufficient to assist the fluid motion and makes the device less sensitive to the aforementioned start-up issues. Most probably, the rising bubbles flatten against the upper side of the tubing and, despite the bubble lift effect being drastically reduced, vapor is able to slide upwards and contribute to convective cooling. Nevertheless, the absence of fluid circulation for all the tested heat inputs results in a higher equivalent thermal resistance with respect to the other inclinations.

As power is increased, equivalent thermal resistance values continue to gradually decrease until a thermal crisis condition is reached, causing temperatures in the affected sections to rise over 100°C, noticeably penalizing thermal performance. When the heat flux locally exceeds the actual CHF, a local dry-out condition occurs meaning that a vapor film prevents heated surface from being rewetted by the liquid. The resulting loss of heat transfer capability in the heated region causes the local temperature to rise abruptly in at least one channel of the device, significantly increasing the equivalent thermal resistance. It is worthwhile to stress that, in case the dry-out occurs, the reported thermal resistance values are approximated and are only qualitatively representing a trend.

Differently form the start-up, a direct relationship between the orientation and the dry-out heat input level is detected for both the symmetrical and the non-symmetrical case: increasing the tilting level towards the horizontal results in a lower value on the heat input capability. It is therefore clear that the gravity head assists the evaporator rewetting: the lower the gravity head, the lower the fluid momentum opposing to the vapor expansion in the down comer, the higher the risk of local dry-out.

3.3 Operational limits and flow regimes

Table 6 shows the different operational regimes observed through the transparent tubing section for both (a) the symmetrical and (b) the non-symmetrical heating at different heat fluxes (yellow x-axis) and inclinations (pink y-axis). The table is divided in two main parts: the left part is referred to the power-up phase, while the right part to the power-down phase. Different operational regimes are recognized and subdivided in four main groups:

- “-“: No fluid motion is detected.
- “S”: all the configurations where a partial start-up occurs. In this case, the heating power is not sufficient to establish a two-phase flow motion along the entire device. As a consequence, it is not possible to define any flow pattern.
- “O”: the oscillating flow, detected after the full start-up. The heating provided is sufficient to establish a net two-phase flow motion through all the channels and the characteristic flow pattern is observable through the transparent section as already shown in Fig. 8a;
- “C”: the fluid circulation. The two-phase flow motion that circulates in a preferential direction, as pointed out previously in Fig. 8c;
- “D”: when dry-out conditions are achieved.

When the test is not performed, the analogous slot in the Table is leaved empty.

Indeed, special attention to the results should be given in terms of heat flux and flow regime maps.

Looking at the power up side, the start up phase for the symmetrical case is less affected by the inclination both in terms of heat flux and flow pattern with respect to the non-symmetrical case, everything runs smoothly from 3.2 W/cm^2 and the flow pattern is always oscillating. The start-up for the non-symmetrical case is more sensitive to inclination even if in a random way (as already said in the previous section), but interestingly its flow pattern is immediately circulating in most of the cases. The circulating flow is maintained until the dry-out condition is reached and also recovered during the power down phase for a wider heat flux range with respect to the symmetric case. However, the non-symmetrical heating pattern is able to withstand higher heat fluxes before the dry-out occurs with respect to the symmetrical case for every inclination from horizontal to 45°: for instance at 45° tilting angle, the symmetrical case stops working between 8.5 and 9.5 W/cm^2 , while the non-symmetrical pattern reaches the dry-out condition between 14.9 and 16.9 W/cm^2. The higher heat flux capability of the non-symmetrical case would be most probably confirmed also for the other orientations if the power supply could cover a wider range. Interestingly enough, if one considers the power down as more representative of the device performance after the full start up, the symmetrical heating case maintains full operation for all the inclinations between 3.2 and 4.6 W/cm^2 while the non-symmetrical case sets its threshold a just bit higher, between 4.2 and 6.4 W/cm^2.

It is important to notice that recovering from the dry-out condition is not a trivial issue: both patterns are able to recover once the heat flux is lowered down, but the crisis phenomenon usually persists at the subsequent heat input levels, and the heat flux must often be decreased by more than one step in order to restore the correct device operation.

4 CONCLUSIONS

A novel concept of advanced multi-evaporator closed loop thermosyphon is tested for two different heating patterns (symmetrical and non-symmetrical) and several orientations in order to assess the beneficial effects of the induced fluid circulation and testify its reliability and very promising thermal performance. The main outcomes are:

- The non-symmetrical heaters layout promotes a stable circulation of fluid in a preferential direction more effectively than the symmetrical case. This is directly observable locally from the glass tube that closes the loop in the condenser zone and also confirmed by the fluid pressure and the wall temperature trends.
- The vertical operation shows the best performance, both in terms of equivalent thermal resistance and heat flux capability. For the non-symmetrical case, in particular, the maximum dissipated heat flux is 75% higher than the Critical Heat Flux for pool boiling of FC-72.
- The device thermal performance and heat power capability is negatively affected by its inclination. Nevertheless, the non-symmetrical case always reaches the dry-out condition at higher heat flux levels with respect to the symmetrical case.
- It is not possible to draw a direct relationship between tilting level and the heat flux level required for the full activation. The non-symmetrical case is more sensitive to the orientation and should be furtherly investigated.
- Orientation directly affects the dry out heat input level is detected both for the symmetric and the non-symmetrical case: increasing the tilting level towards the horizontal results in a lower value on the heat input capability.
- The system is able to recover from the dry-out condition but the crisis phenomenon usually persists at the lower heat input levels, and the heat flux must be decreased to some extent more, in order to restore the correct device operation.

Being passive, light, relatively flexible in terms of shape and surface adaptability, more effective with respect to TS, having no entrainment limits, and more reliable for the time being of a PHP, the MELT represents a breakthrough, compact and flexible passive solution towards energy saving in many thermal management applications.

NOMENCLATURE

A_e	Wall to Fluid Evaporator Surface,	[m^2]
Bo	Bond Number,	[-]
Δh_{lv}	Latent heat of vapor,	[J/kg]
d_{in}	Tube diameter,	[m]
FR	Filling ratio,	[-]
g	Gravity Acceleration,	[m/s2]
I	Current	[A]
Ku	Kutateladze Number,	[-]
l_c	Capillary Length,	[m]
l_e	Evaporator Length,	[m]
q''	Wall to Fluid Heat Flux,	[W/cm^2]
q''_{CHF}	Critical Heat flux,	[W/cm^2]
$\dot{Q}$	Heat Input Power	[W]
$\dot{Q}_{CHF}$	Maximum Heat Input Power,	[W]
R_{el}	Electric resistance	[Ohm]
R_{th}	Thermal Resistance,	[K/W]
ρ_l	Liquid Density,	[kg/m^3]
ρ_v	Vapor Density,	[kg/m^3]
σ	Surface Tension ,	[N/m]
σ_e	Temperature standard deviation evaporator,	[°C]
σ_c	Temperature standard deviation condenser,	[°C]
φ	Inclination angle	[deg]
$\bar{T}$	Average Temperature ,	[°C]
T_i	Evaporator Ith termperature	[°C]
δT_{ds}	Temperature uncertainty from datasheet	[°C]
TC	Thermocouple,	[-]

ACKNOWLEDGEMENTS

The present work has been carried out in the framework of the Italian Space Agency (ASI) project ESA_AO-2009 entitled “Innovative two-phase thermal control for the International Space Station”. The authors would like to thank Dr. Olivier Minster and Dr. Balazs Toth of the European Space Agency for their interest and support to the PHP activities and for the fruitful discussions. Also we acknowledge Ing. Paolo Emilio Battaglia of the Italian Space Agency for his administrative support. Ing. Davide Fioriti for his precious support on the Data Acquisition side. Finally we thank all the members of the Pulsating Heat Pipe International Scientific Team, for their contribution in pushing the PHP technology for space applications, with a particular gratitude to Prof. Sameer Khandekar, Dr. Vadim Nikolayev, Dr. Vincent Ayel and Prof. Marcia Mantelli.

REFERENCES

[1] Stocker T.F. et al., Climate Change 2013: The Physical Science Basis. Contribution of Working Group I to the Fifth Assessment Report of the Intergovernmental Panel on Climate Change, Cambridge University Press, Cambridge, UK and New York, NY, USA.

[2] Schmidt, R. and Iyengar, M., Thermodynamics of Information Technology Data Centers, IBM J. Res. & Dev 2009, Vol. 53, No. 3, Paper 9.

[3] Lahey R.T, Moody F.J. 1993, Thermal Hydraulic of Boiling Water Nuclear Reactor, American Nuclear Society.

[4] Franco A., Filippeschi S., Experimental analysis of Closed Loop Two Phase Thermosyphon (CLTPT) for energy systems, Exp. Thermal and Fluid Science 2013; 51:302–311.

[5] Esen M., Esen H., Experimental investigation of a two-phase closed thermosyphon solar water heater. Solar Energy 2005; 79:459-468.

[6] Li J., Lin F., Niu G., An insert-type two-phase closed loop thermosyphon for split-type solar water heaters. Applied Thermal Eng. 2014; 70:441-450.

[7] Moradgholi M., Nowee S. M., Abrishamchi I., Application of heat pipe in an experimental investigation on a novel photovoltaic/thermal (PV/T) system. Solar Energy 2014; 107:82-88.

[8] Han L., Shi W., Wang B., Zhang P., Li X., Development of an integrated air conditioner with thermosyphon and the application in mobile phone base station. Int. J. of Refrigeration 2013; 36:58-69.

[9] Sarno C., Tantolin C., Hodot R., Maydanik Y., Vershinin S., Loop thermosyphon thermal management of the avionics of an in-flight entertainment system, App. Ther. Eng. 2013; 51:764-769.

[10] Perpinà X., Piton M., Mermet-Guyennet M., Jorda` X., Millàn J., Local thermal cycles determination in thermosyphon-cooled traction IGBT modules reproducing mission profiles. Microelectronics Reliability 2007; 47:1701–1706.

[11] Reay D.A., Kew P.E., Heat Pipes, 2006, Fifth ed., Butterworth-Heinemann, Burlington, USA.

[12] Bezrodnyy M. K., Volkov S. S., Alekseyenko D. V., Maximum Heat Transfer in Thermosyphons with Separated Uptake and Downtake, Heat Transfer Soviet Research, 1983; 15(2): 108-114.

[13] Franco A., Filippeschi S., Closed Loop Two-Phase Thermosyphon of Small Dimensions: a Review of the Experimental Results, Microgravity Sci. Technol. 2012; 24:165–179.

[14] Franco A., Filippeschi S., Experimental analysis of heat and mass transfer in small dimension, two phase loop thermosyphons, Heat Pipe Science and Technology 2010; 2:163–182.

[15] Zhang Y. , Faghri A.,. Advances and Unsolved Issues in Pulsating Heat Pipes. *Heat Transfer Engineering*, 2009; 29(1):20-44.

[16] Han X., Wang X., Zheng W., Xu X., Chen G., Review of the development of pulsating heat pipe for heat dissipation, Renewable and Sustainable Energy Reviews, 2016; 59:692–709.

[17] Kim C. J., Yoo B. O., Park Y. J., Experimental Study of a Closed Loop Two-Phase Thermosyphon with Dual Evaporator in Parallel Arrangement. Journal of Mech. Sci. and Tech. 2005; 19(1):189-198.

[18] Kaminaga F., Matsumura K., Horie R., Takahashi A., A Study on Thermal Conductance in a Looped Parallel Thermosyphon, 16th International Heat Pipe Conference, Lyon, France, May 20-24, 2012.

[19] Jouhara H., Robinson A. J., Experimental investigation of small diameter two-phase closed thermosyphons charged with water, FC-84, FC-77 and FC-3283. App. Ther. Eng. 2010; 30:201–211.

[20] Mameli M., Manno V., Filippeschi S., Marengo M., Thermal instability of a Closed Loop Pulsating Heat Pipe: Combined effect of orientation and filling ratio. Exp. Ther. and Fluid Sci. 2013; 59:222–229.

[21] Henry C. D., Kim J., Chamberlain B., Heater size and heater aspect ratio effects on sub-cooled Pool boiling heat transfer in low-g 3rd International Symposium on Two-Phase Flow Modeling and Experimentation Pisa, 22-24 September, 2004.

[22] Moffat, R.J., Describing the Uncertainties in Experimental Results, Experimental Thermal and Fluid Science 1988; 1: 3-17.

[23] Golobic I., Gaspersic B., Corresponding States Correlation for Maximum Heat Flux in Two Phase Closed Thermosyphon, *Int. J. Refrig. 1997; 20(6):402-410*.

[24] Kutateladze S.S. A Hydrodynamic Theory of Changes in the Boiling Process Under Free Convection Condition, Izv. Akad. Nauk. SSSR Odt. Tehk. Nauk 1951; 4:529,536.

[25] Zuber, N., Hydrodynamic Aspects of Boiling Heat Transfer, AEC Report No. AECU-4439, Physics and Mathematics 1959.

[26] Katto Y., Generalized Correlation for Critical Heat Flux of the Natural Convection Boiling in Confined Channels, Trans. Japan Soc. Mech. Engrs. 1978; 44:3908-3911.

[27] Pioro I. L., Voroncova M.V., Rascetnoe Opredelenie Predelnogo Teplovogo Potoka Pri Kipienii Zidkostej v Dvuhfaznih Termosifonah, Inz. Fiz. Zurnal 1987; 53:376-383.

[28] Jung J., Kim S. J., Kim J., Observations of the Critical Heat Flux Process During Pool Boiling of FC-72, J. of Heat Transfer 2014; Vol.136. DOI: 10.1115/1.4025697.

List of Tables

Table 1. Advantage (green) and drawbacks (red) of the wickless heat pipe technologies.

	Counter-Flow Thermosyphon (TS)	**Multi-Evap. Loop Thermosyphon (MELT)**	**Pulsating Heat Pipe (PHP)**
3D space adaptability	LOW	HIGH	VERY HIGH
Thermally controlled surface	MEDIUM	HIGH	VERY HIGH
Dependency on gravity assistance	VERY HIGH	HIGH	LOW
Heat flux capability	MEDIUM	VERY HIGH	MEDIUM
Operation reliability	VERY HIGH	HIGH	MEDIUM
Modeling/Design tools	HIGH	LOW	LOW
Cost	LOW	LOW	LOW

Table 2: Heater layouts characteristics

Layout	l_e [mm]	A_e [cm^2]	$\dot{Q}$ [W]	q” [W/cm^2]
Symmetrical	40	3.8	10 - 260	1.06 - 27.5
Non symmetrical	20	1.9		0.53 – 13.75

Table 3: Uncertainties a) from datasheet; b) calculated on the different heat input steps for the non-symmetrical configuration, vertical case.

a) FROM DATASHEET		
δT_{ds}	δR_{el}	δI
0.86 °C	0.2 Ohm	0.03 A

b)	CALCULATED AT EACH POWER STEP								
$\dot{Q}$[W]	$\delta\dot{Q}$[W]	$\frac{\delta\dot{Q}}{\dot{Q}}\%$	$\bar{T}_e$[°C]	$\delta\bar{T}_e$[°C]	$\bar{T}_c$[°C]	$\delta\bar{T}_c$[°C]	R_{th}[K/W]	δR_{th}[K/W]	$\frac{\delta R_{th}}{R_{th}}\%$
10	0.58	5.80	25.99	0.39	19.99	0.36	0.60	0.06	10.55
20	0.91	4.55	30.69	0.41	20.90	0.36	0.49	0.04	7.19
30	1.21	4.03	36.19	0.41	21.76	0.36	0.48	0.03	5.51
40	1.50	3.75	34.72	0.42	23.57	0.36	0.28	0.02	6.22
60	2.07	3.45	39.14	0.40	25.89	0.36	0.22	0.01	5.31
90	2.90	3.22	45.15	0.40	29.48	0.36	0.17	0.01	4.71
120	3.73	3.11	51.00	0.41	33.30	0.36	0.15	0.01	4.37
160	4.83	3.02	58.17	0.42	38.08	0.36	0.13	0.01	4.09
210	6.21	2.96	67.56	0.42	44.28	0.36	0.11	0.00	3.78
260	7.58	2.92	77.54	0.43	50.59	0.37	0.10	0.00	3.58

Table 4. Critical Heat Flux Correlations.

CASE, [References]	**Correlation**	**Ku**	**q''_{CHF} [W/cm^2]**
Pool boiling on large finite surfaces, Zuber [25]	$Ku = \pi/24$ (3)	0.131	**16.4**
Pool boiling in confined channels, Katto [26]; Pioro and Voroncova [27]	$Ku = 0.1/\left[1+0.491\left(l_e/d_{in}\right)Bo^{-0.3}\right]$ (4) Where $Bo = g\left(\rho_l-\rho_v\right)d_{in}^{\,2}/\sigma$ $Ku = 0.131\left\{1-\exp\left[-\left(\frac{d_{in}}{l_e}\right)\left(\frac{\rho_l}{\rho_v}\right)^{0.13}\cos^{0.18}\left(\varphi-55°\right)\right]\right\}^{0.8}$ (5)	0.043; 0.041	**5.4;** **5.2**

Table 5. Comparison between different technologies.

5 CASE	**Closed Thermosyphon (TS)**	**Multi-Evap. Loop Thermosyphon (MELT)**	**Pulsating Heat Pipe (PHP)**	**Pool Boiling**
Reference	Jouhara and Robinson [19]	Present work	Mameli et al. [20]	Jung et al. [28]
Fluid	FC-84	FC-72	FC-72	FC-72
FR (Vol.)	0.25	0.50	0.50	-
Fluid Vol. [ml]	1.8	5.6	3.1	-
d_{in} [mm]	6.0	3.0	1.1	-
l_{tot} [m]	0.2	0.2	0.2	-
l_e [m]	0.05	0.02	0.015	
N° of heated sections	1	5	16	1
A_e [cm2]	9.42	9.42	8.53	4
$\dot{Q}_{CHF}$ [W]	50	260	90	62.8
q”$_{CHF}$ [W/cm2]	**5.31**	**27.59**	**10.55**	**15.7**
R_{th} [K/W]	1.0	0.1	0.2	-
MELT improvement [%]	520	-	261	175

Table 6. Flow pattern maps: a) Symmetrical case; b) Non-symmetrical case.

a) SYMMETRICAL HEATING																										
	Power-up phase (Q-up)													Power-down phase (Q-down)												
90°	-	-	-	S	O	O	O		O		C		C		C		O		O	O	O	S	-	-	-	90°
75°	-	-	-	-	O	O	O		C	C	C		C		C	C	C		O	O	O	O	O	-	-	75°
60°	-	-	-	-	O	O	O		C	C	C	C	C	C	C	C	C		O	O	O	S	S	-	-	60°
45°	-	-	O	O	O	O	O		O	D							D		O	O	O	S	S	-	-	45°
30°	-	-	S	O	O	O	O	D										D	O	O	S	-	-	-	-	30°
15°	-	-	S	S	O	O	D												D	O	O	O	O	-	-	15°
2.5°	-	S	S	S	O	D														D	O	O	O	S	-	2.5°
0°	-	-	-	-	-	-														-	-	-	-	-	-	0°
q”[W/cm2]	0.5	1.0	1.6	2.1	3.2	4.8	6.4	7.4	8.5	9.5	11.1	12.7	13.8	12.7	11.1	9.5	8.5	7.4	6.4	4.8	3.2	2.1	1.6	1.0	0.5	q”[W/cm2]
P[W]	10	20	30	40	60	90	120	140	160	180	210	240	260	240	210	180	160	140	120	90	60	40	30	20	10	P[W]

b) NON SYMMETRICAL HEATING																								
	Power-up phase (Q-up)												Power-down phase (Q-down)											
90°	-	-	S	C	C	C	C		C		C	C	C		C		C	C	C	C	O	S	S	90°
75°	-	-	S	S	S	S	C		C	C	D				D		C	C	C	O	S	S	-	75°
60°	-	-	-	C	C	C	C		C	C	D				D		C	C	O	O	S	S	-	60°
45°	-	-	-	-	O	C	C		D						D		C	C	C	O	S	S	-	45°
30°	-	-	-	-	C	C	C	D								D	O	C	C	O	-	-	-	30°
15°	-	S	S	S	S	O	D										D	O	O	S	S	S	-	15°
2.5°	-	O	O	O	D	D												D	O	O	O	-	-	2.5°
0°	-	-	-	-	-	-												-	-	-	-	-	-	0°
q”[W/cm2]	1.0	2.1	3.2	4.2	6.4	9.6	12.7	14.9	16.9	19.1	22.3	27.6	22.3	19.1	16.9	14.9	12.7	9.6	6.4	4.2	3.2	2.1	1.0	q”[W/cm2]
P[W]	10	20	30	40	60	90	120	140	160	180	210	260	210	180	160	140	120	90	60	40	30	20	10	P[W]

List of Figures

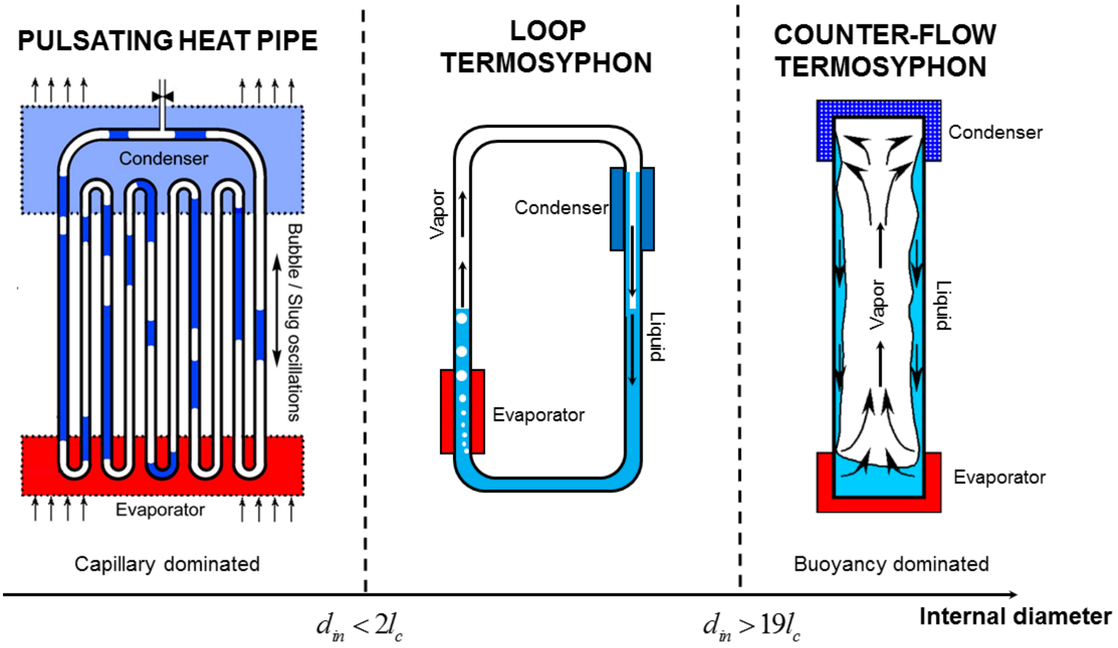

Figure 1: Wickless Heat Pipes working principles in the light of the confinement criteria [14].

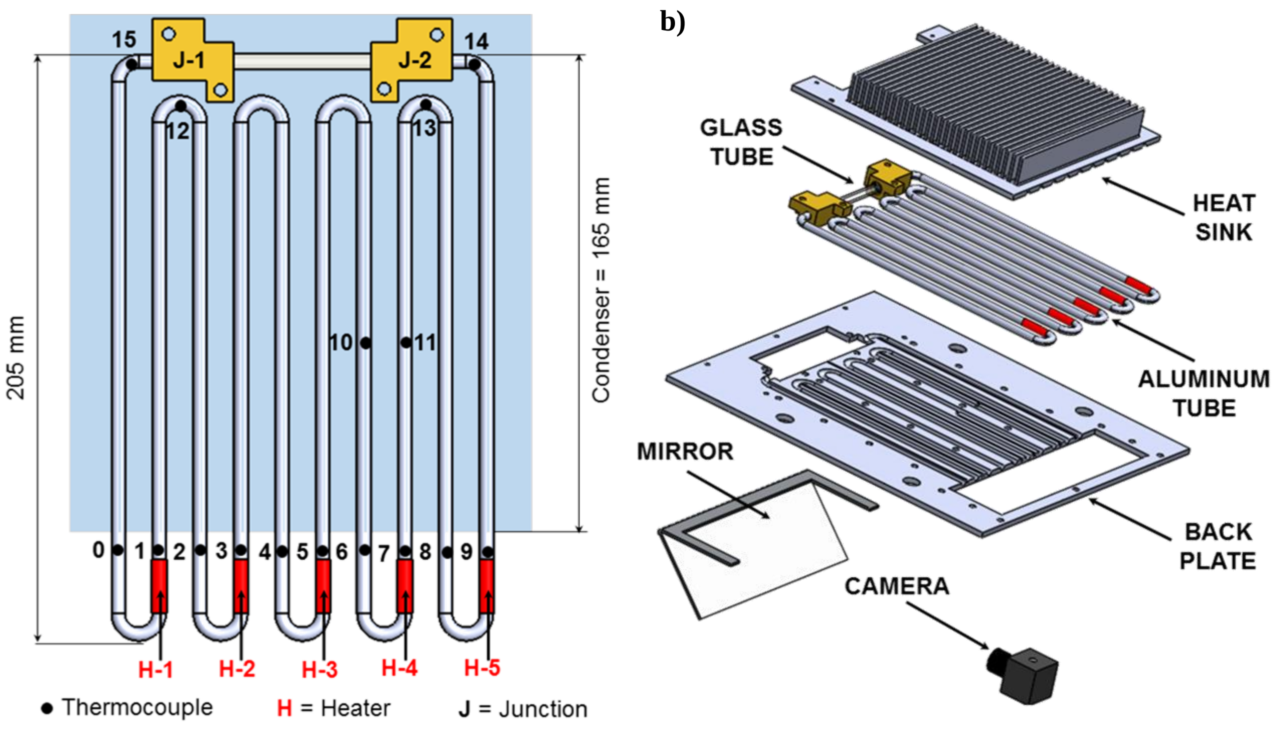

Figure 2. a) Thermocouples and heaters location (non-symmetrical case); b) Exploded view of the test cell. To notice is the position of TC14 and TC15 at the boundaries of the transparent tube insert.

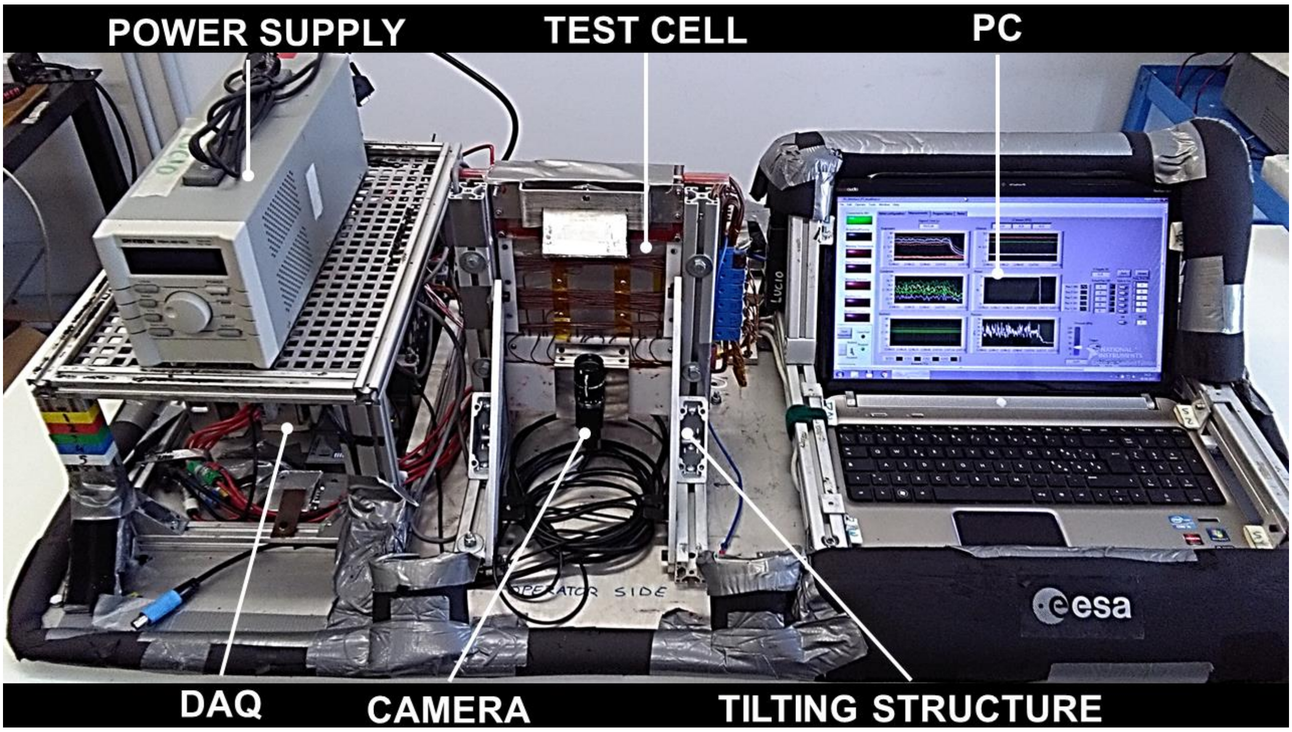

Figure 3: Test rig and main components.

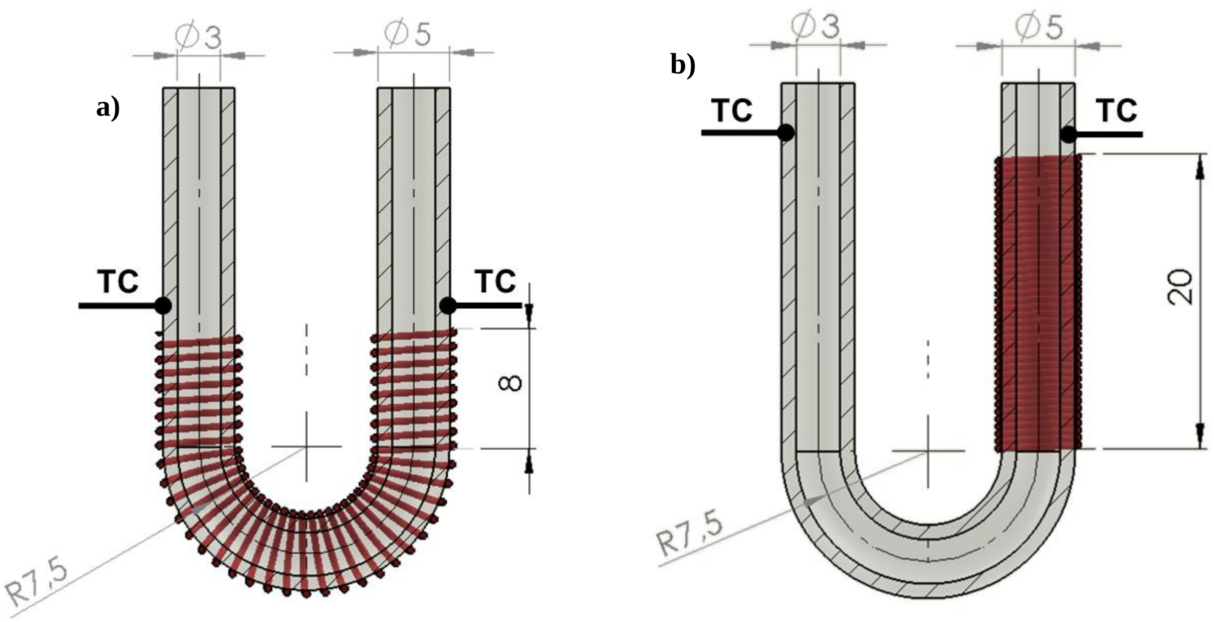

Figure 4: Heater and thermocouples arrangements, a) symmetrical, b) non-symmetrical.

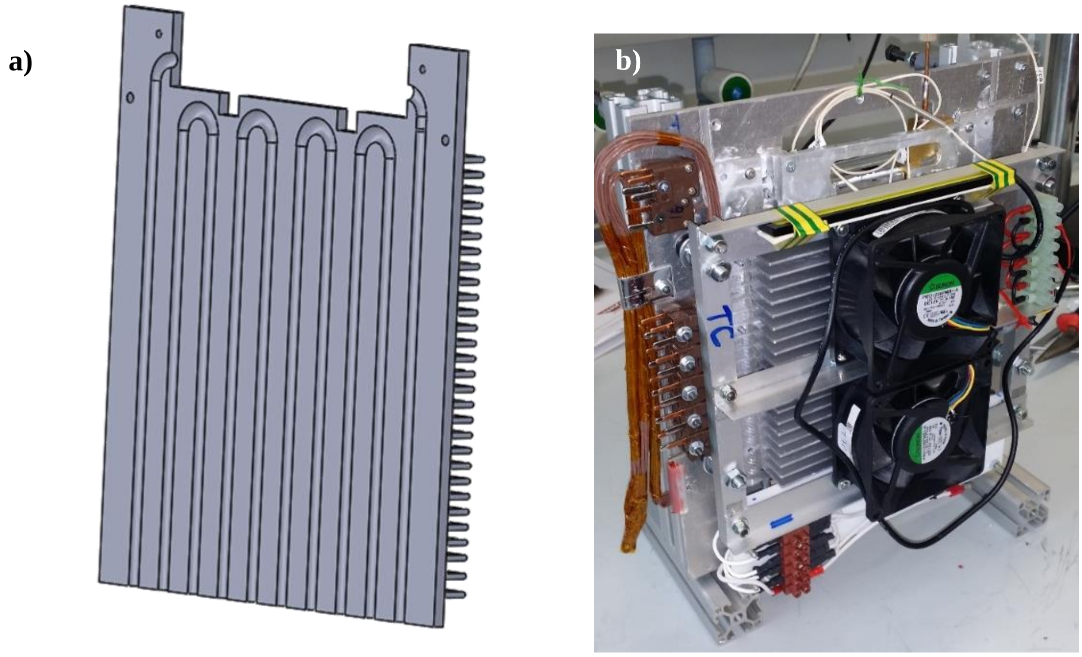

Figure 5. a) CAD view of the milled heat sink; b) The two fans mounted above the heat sink.

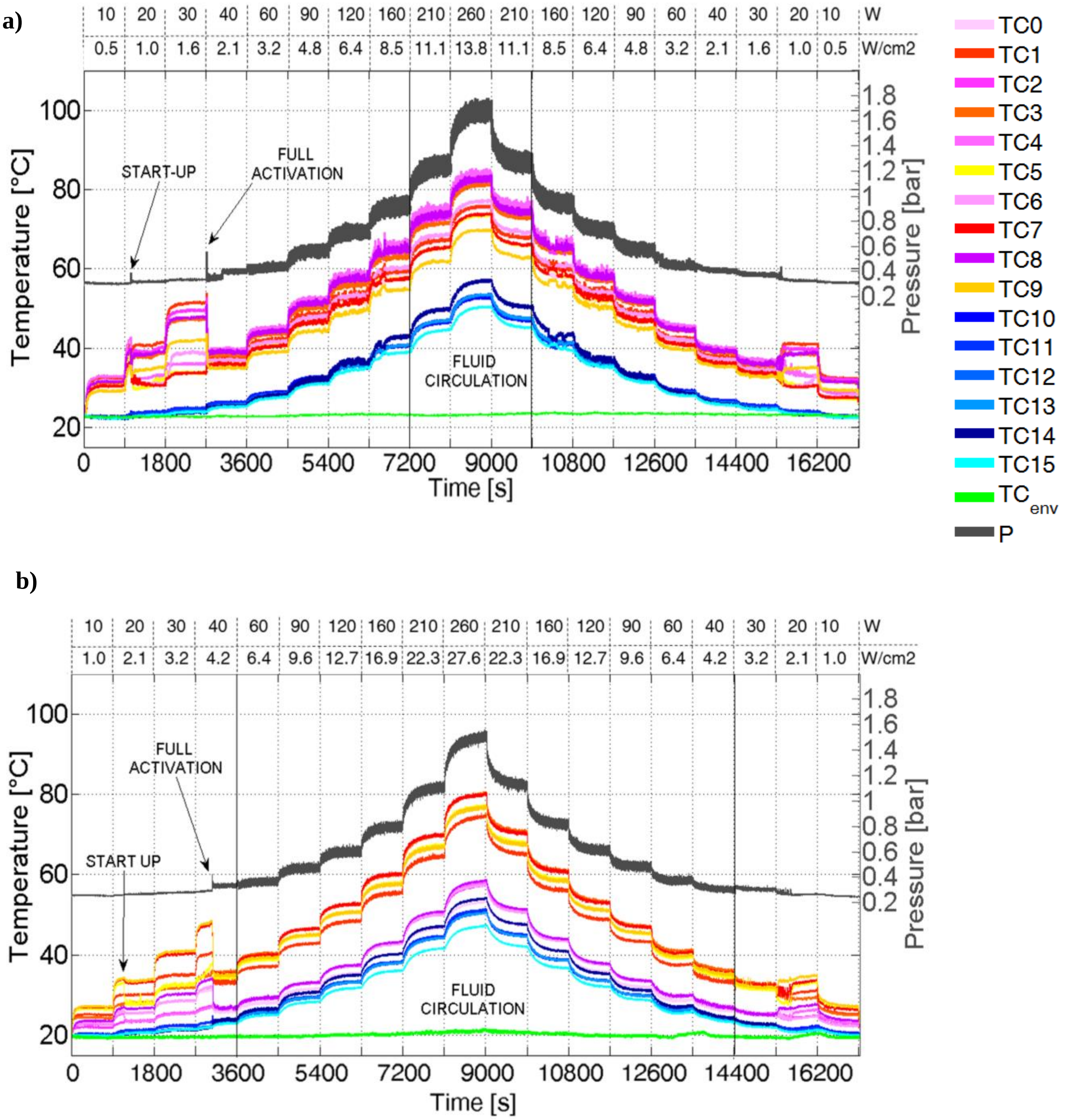

Figure 6. Temperature, pressure and power input diagram in vertical position, a) symmetrical heating; b) non symmetrical heating.

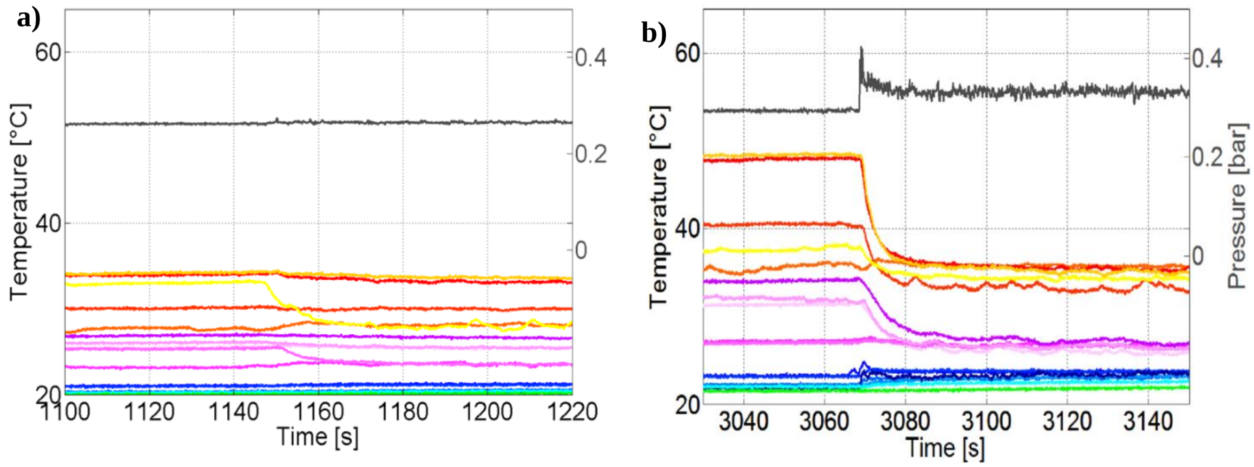

Figure 7: Wall temperature and fluid pressure: a) partial startup at 20W; b) Complete activation at 40W.

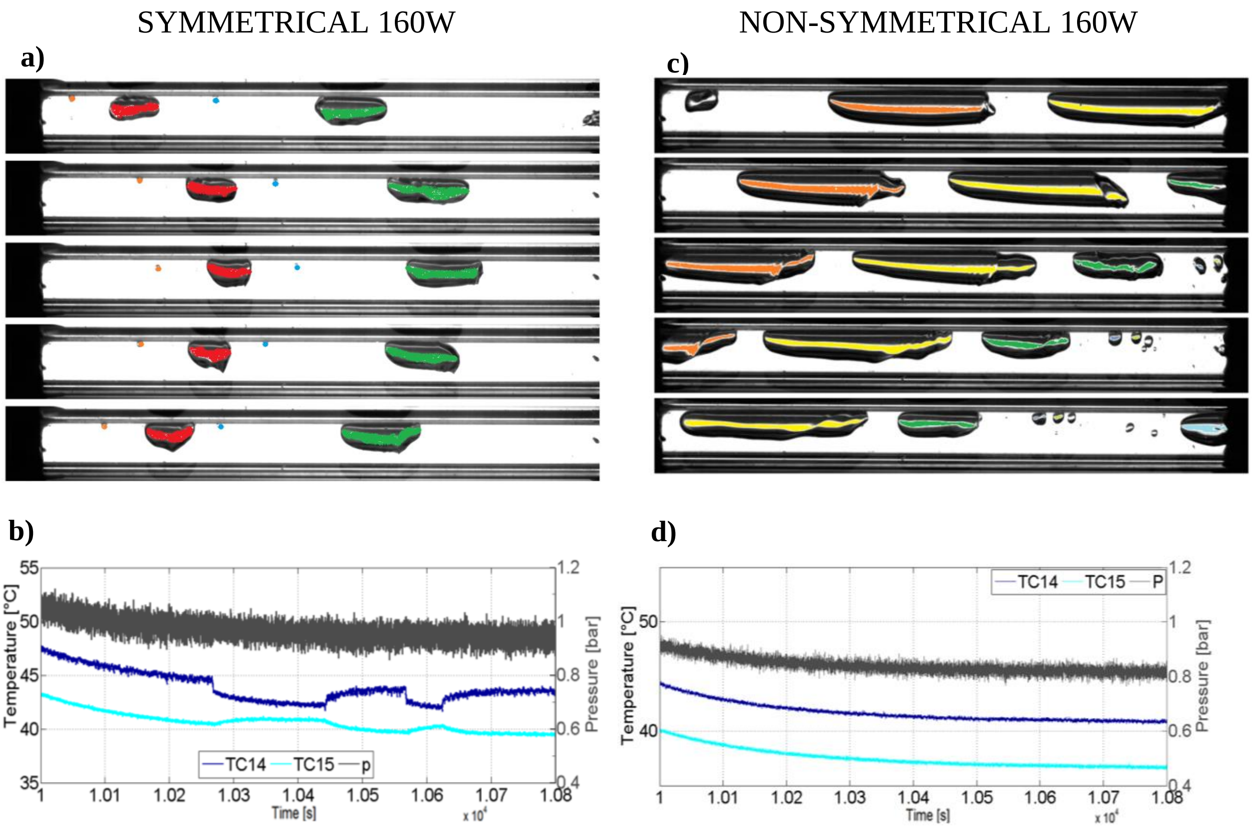

Figure 8. Symmetrical, a) visualization of oscillating motion 45 fps; b) Temperature and Pressure measurements at the transparent section ends; Non-Symmetrical, c) visualization of oscillating motion 45 fps; d) Temperature and Pressure measurements at the transparent section ends.

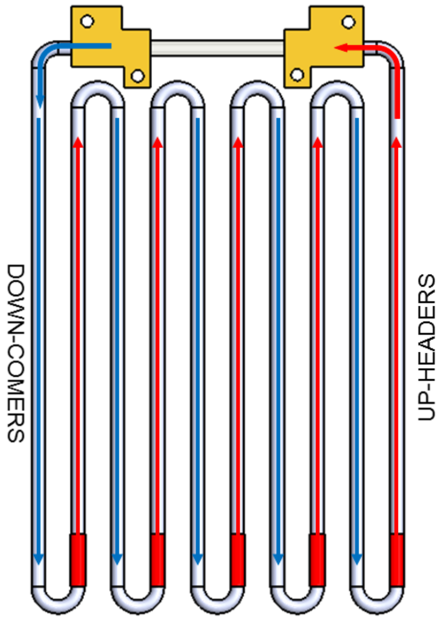

Figure 9: Fluid circulation scheme with up-headers (red arrows) and down-comers (blue arrows).

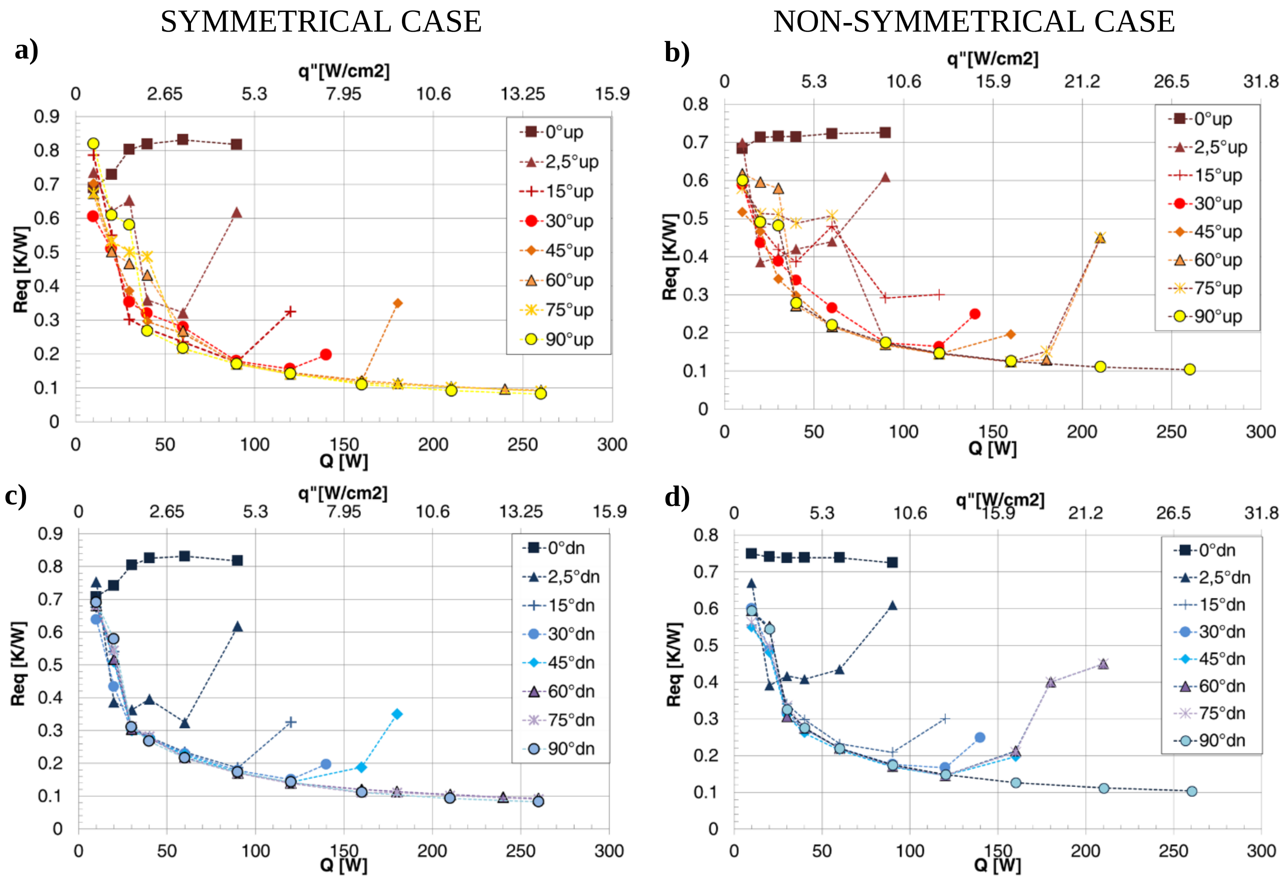

Figure 10. Equivalent thermal resistance for the various inclinations. The first power-up: a) symmetrical case, b) non-symmetrical case; the subsequent power-down: c) symmetrical case, d) non-symmetrical case.